DTU Library

Bistable switching in supercritical n+-n-n+GaAs transferred electron devices

Jøndrup, Peter; Jeppesen, Palle; Jeppson, Bert

Link back to DTU Orbit

Bistable Switching in Supercritical n⁺-n-n⁺ GaAs Transferred Electron Devices

PETER JØNDRUP, PALLE JEPPESEN, MEMBER, IEEE, AND BERT JEPPSSON

Abstract—Bistable switching in supercritically doped n⁺-n-n⁺ GaAs transferred electron devices (TED's) is investigated experimentally and interpreted in computer simulations, for which details of the computer program are given. Three switching modes all leading to stable anode domains are discussed, namely: 1) cathode-triggered traveling domain; 2) cathode-triggered accumulation layer; 3) anode-triggered domain. Relative current drops up to 40 percent, and switching times down to 60 ps are obtained in low-duty-cycle pulsed experiments with threshold currents around 400 mA. Optimum device parameters are shown to be as follows: 1) doping in the 3–4 × 10¹⁵ cm⁻³ range; 2) length around 6 μm; 3) doping gradients below 20 percent; 4) high-quality interfaces.

I. INTRODUCTION

THIS PAPER presents an experimental investigation showing that supercritically doped n⁺-n-n⁺ GaAs transferred electron devices (TED's) can be used as fast bistable switches with current drops up to 40 percent and switching times down to 60 ps. The experimental results will be interpreted in simple physical terms by comparison with computer simulations. Finally, the optimum device parameters for such a Gunn switch will be defined.

Bistable switching due to formation of a diffusion stabilized anode domain has been predicted theoretically [1] and verified experimentally by Thim [2]. The switching takes place in 60–120 ps between a high current state below the threshold voltage and a low current state above threshold. In the following those two stable states will be denoted the off- and on-state, respectively. The subthreshold off-state is trivial, while the on-state is characterized by the presence of a diffusion stabilized domain frozen at the anode.

Before discussing the bistable Gunn switch any further, a few remarks on two different types of stability are relevant. Short-circuit stability in TED's may be divided into two basic types [3]:

1) stability due to the presence of a diffusion stabilized anode domain in heavily doped devices with ohmic contacts [4];
2) stability when the product of doping and length is below a certain critical value [5].

Devices with stability of type 2) may have favorable noise and linearity behavior in microwave reflection-type amplifiers [6], but they are besides the scope of the present paper, because only devices with type 1) stability exhibit bistable switching.

In Section II the bistable switching will be investigated using large-signal computer simulations, and the results will be interpreted in simple physical terms. Section III presents experimental results and defines the optimum parameters for the Gunn switch. Section IV contains the conclusion and discussion.

II. COMPUTER SIMULATIONS

A. Formulation of the Model

The computer simulations are based on the Poisson equation

$$\frac{\partial E}{\partial x} = \frac{q}{\epsilon}(n - n_0) \tag{1}$$

and the continuity equation

$$J(t) = qnv - q\frac{\partial}{\partial x}(Dn) + \epsilon\frac{\partial E}{\partial t} \tag{2}$$

where $E(x,t)$ is the space- and time-dependent electric field, $n(x,t)$ is the free electron density, n_0 is the net donor density in the active layer, $-q(q > 0)$ is the electronic charge, ϵ is the absolute permittivity of GaAs, $J(t)$ is the space independent total current density, $v(E)$ is the electron drift velocity—electric field characteristic, and $D(E)$ is the electron diffusion coefficient—electric field characteristic in GaAs. The $v(E)$—and $D(E)$—curves used in the present work are shown in Fig. 1, and are similar to curves used in earlier work [7] except for the fact that the subthreshold portion of the $v(E)$ curve has been taken to be more linear in agreement with current–voltage $(I–V)$ measurements performed on the actual devices used in this work. In the interest of saving computer time, also the steady-state equations—following from (1) and (2) by setting $\partial/\partial t$ terms equal to zero—were solved in particular cases. Numerical integration procedures are summarized in Appendices A and B.

B. Space-Charge Dynamics

The switching from the off- to the on-state may take place in different ways. In large-signal time-dependent computer simulations the following three space-charge
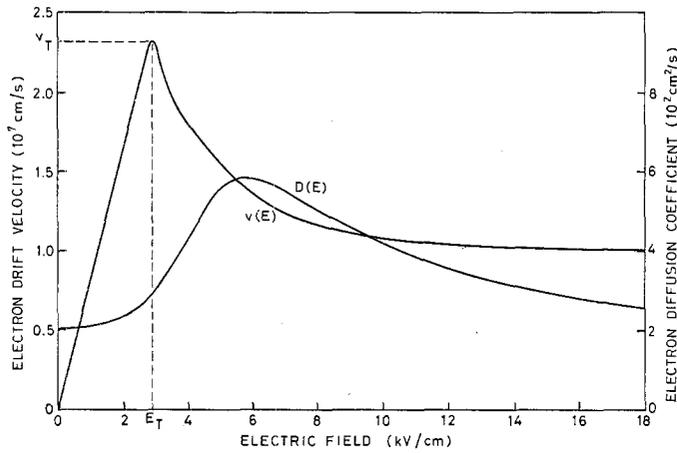
Fig. 1.   Room temperature $v(E)$ and $D(E)$ curves used in computer simulations.
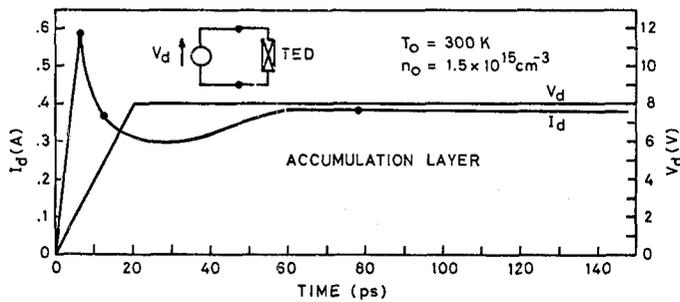

Fig. 2.   Applied voltage V_d and electronic current I_d versus time for GaAs TED switching in traveling accumulation layer mode. Device data: $n_0 = 1.5 \times 10^{15}$ cm^{-3}, $L_a = 10$ μm, $R_0 = 5$ Ω, $T_0 = 300$ K.

(a)

(b)

(c)

Fig. 3.   Calculated electric field (E) and electron density profile (n) for device in Fig. 2. (a) Off-state. (b) During switching. (c) On-state.

modes have been observed when the device voltage exceeds the threshold value.

1) A dipole domain is triggered at the cathode, travels towards the anode, where it is trapped as a stable high field domain.

2) An accumulation layer is triggered at the cathode, travels towards the anode, where it readjusts into a stable high field domain.

3) The instability is triggered directly at the anode, where it grows and then settles as a stable high field domain.

In qualitative agreement with a small-signal analysis by Guéret [8], space-charge modes 1) and 2) stem from convective instabilities triggered at the cathode and occur for the lower doping levels ($n_0 = 1$–2×10^{15} cm^{-3}), while space-charge mode 3) stems from an absolute instability and is encountered for higher doping levels ($n_0 > 3 \times 10^{15}$ cm^{-3}).

In case the instability is triggered at the cathode, it will grow either to an accumulation layer or a full domain depending mainly on the magnitude of the doping nonuniformity and the rise time of the applied voltage. For the sake of brevity we omit the dipole domain for the moment. Figs. 2 and 3 illustrate the switching mode involving a traveling accumulation layer. Fig. 2 shows the applied voltage V_d and the calculated electronic current I_d for a switch having the active layer thickness
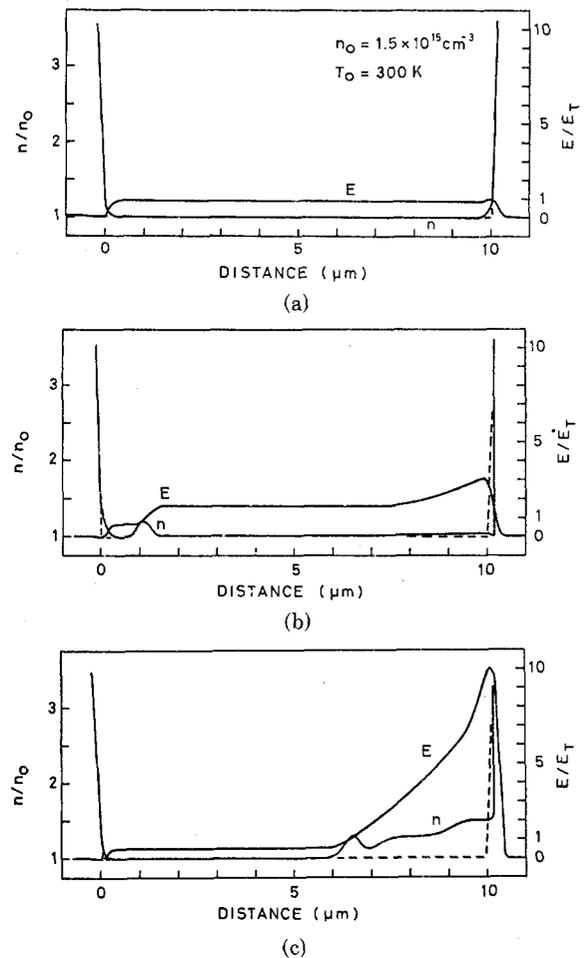
$L_a = 10$ μm, the doping density $n_0 = 1.5 \times 10^{15}$ cm^{-3}, the low field resistance $R_0 = 5$ Ω, the lattice temperature $T_0 = 300$ K, and a flat and smooth doping profile. The voltage was applied with a rise time $\tau_R = 20$ ps, and such a short rise time was normally used in the interest of saving computer time and because it did not affect the results in any essential way as could be concluded from comparisons with similar runs using an order of magnitude longer rise times. Fig. 3 shows snapshots of the electric field profile E and electron density profile n, at the time instants indicated by the dots on the calculated current waveform in Fig. 2. Here E_T denotes the threshold electric field (Fig. 1). Fig. 3(a)–(c) illustrates the profiles in the off-state, during switching and in the on-state, respectively. In the on-state the field is characterized by a diffusion stabilized high field domain frozen at the anode. Figs. 4 and 5 illustrate the switching mode involving an anode instability. Here all the parameters are the same as before, except that the doping level is increased to 3×10^{15} cm^{-3}.

In case of a cathode-triggered instability (dipole domain or accumulation layer), Fig. 2 shows that two time constants determine the time necessary for I_d to become stable: 1) the time constant for the initial decay of I_d, i.e., the negative dielectric relaxation time control-
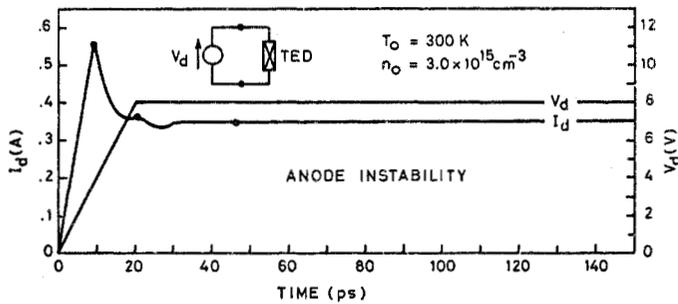
Fig. 4. Applied voltage V_d and electronic current I_d versus time for GaAs TED switching due to absolute anode instability. Device data: $n_0 = 3.0 \times 10^{15}$ cm^{-3}, $L_a = 10$ μm, $R_0 = 5$ Ω, $T_0 = 300$ K.

Fig. 6. Calculated relative current drop versus doping density. Device data: $L_a = 10$ μm, $R_0 = 5$ Ω, $T_0 = 300$ K. Circuit data: $V_B = 8.0$ V, $\tau_R = 20$ ps. Solid curve: flat and smooth doping profile. Dashed curve: 10 percent random doping fluctuations.

ly, the current drop ΔI is defined by

$$\Delta I = I_T - I_{ds}$$

where I_{ds} is the device saturation current and I_T is the threshold current given by

$$I_T = Aqn_0 v_T.$$

Here A is the cross-sectional area and $v_T = v(E_T)$ is the peak velocity (Fig. 1).

C. Influence of Basic Device Parameters

In this section we discuss the influence of basic device parameters—such as length and doping level—on the current drop of the bistable Gunn switch.

The computer simulations have shown that the current in the on-state is independent of the length of the active layer, provided the doping profile is smooth and flat. This can be understood from Figs. 3 and 5, which show that the field in front of the stable domain is flat, meaning that one can add or remove a section of the diode in front of the domain without changing the current in the on-state. Since the threshold current would also be independent of such a change, it is concluded that the current drop is independent of the active layer length, as long as this length exceeds the domain width. In the following we shall consider a typical length of about 10 μm. Further, the computer simulations have also shown that the on-state current is independent of the bias voltage, simply because an increased voltage only causes a broader domain but not a different field in front of the domain. The independence of the current drop on length and bias voltage has been found in an earlier analytical treatment [4].

The most important parameter for the current drop is the doping density. Fig. 6 shows the relative current drop $\Delta I/I_T$ versus doping density. As before, the voltage was applied with a rise time $\tau_R = 20$ ps and then kept constant at $V_B = 8.0$ V. The current drop was determined on the basis of electronic current in order to avoid irrelevant contributions from possible capacitive overshoot in the total current. As seen from Fig. 6, the relative current drop increases with doping density and values up to about 40 percent are predicted for a flat and smooth doping profile. However, 10 percent ran-
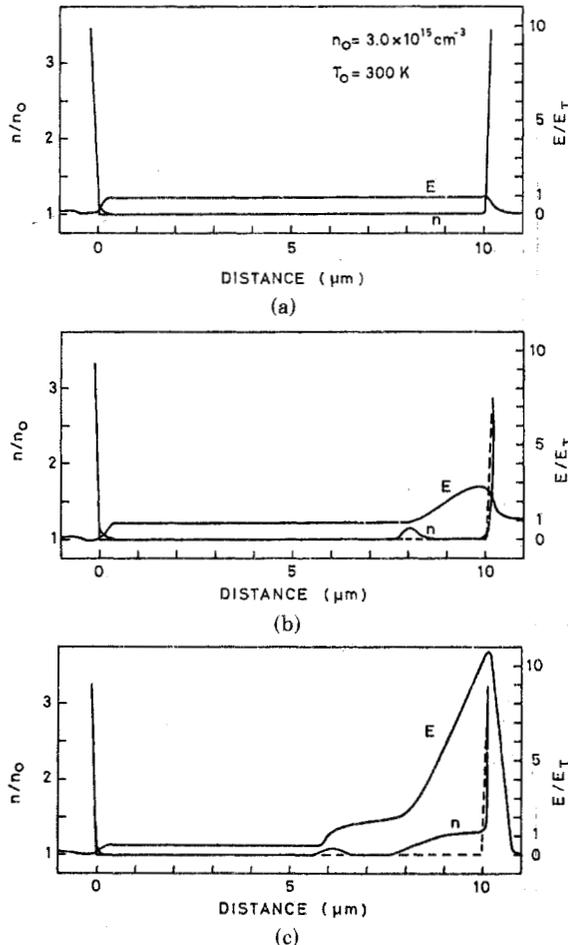

Fig. 5. Calculated electric field (E) and electron density profile (n) for device in Fig. 4. (a) Off-state. (b) During switching. (c) On-state.

ling the speed of growth for the instability; and 2) the transit time for the space-charge layer to travel from cathode to anode. For the anode-triggered absolute instability there is no space-charge layer in transit, and, hence, no transit time involved; I_d becomes stable already after the domain growth time mainly determined by the negative dielectric relaxation time. Therefore this switching mode offers the potentially fastest Gunn switch. Finally, it should be noted that for a given set of device parameters the final current drop is independent of the three switching modes because the initial and final states are the same in all three cases. Quantitative-
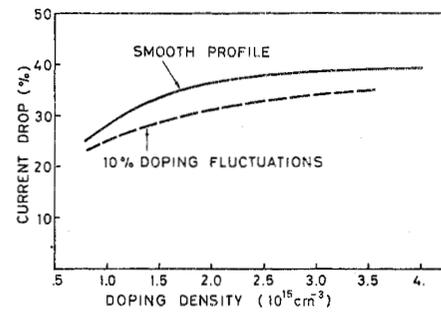
Fig. 7. Calculated dc I-V curve. Device data: $n_0 = 3.0 \times 10^{15}$ cm^{-3}, $L_a = 10$ μm, $R_0 = 5$ Ω, $T_0 = 300$ K. Solid curve: flat and smooth doping profile. Dotted curve: -20 percent doping gradient (decreasing towards anode). Dashed curve: $+20$ percent doping gradient (increasing towards anode).

dom doping fluctuations reduce the current drop, because nonuniformities in the doping profile reduce the peak current in the off-state to a value somewhat below the threshold current I_T.

Although the detrimental effect of doping fluctuations is thus clear, the effect of doping gradients is more serious and of larger practical significance. Fig. 7 illustrates the influence of doping gradients on the dc I-V characteristic. Here a positive (negative) doping gradient indicates a profile sloping upward (downward) towards the anode. As seen from Fig. 7, the threshold current I_T is never reached in the presence of doping gradients, obviously because a small domain is already formed below threshold either at the cathode or anode, depending on whether the gradient is positive or negative. In the on-state the current is lowest for the negative gradient, because it turns out that the anode domain assumes such a high peak field and therefore absorbs so much voltage, that the field in front of the domain is reduced. The opposite situation occurs for a positive gradient. Moreover, Fig. 7 shows that both the positive and the negative gradient give a current drop smaller than for the case of a flat profile.

In the case of steep doping gradients (in the 50–100 percent range) the performance of the Gunn switch will be strongly degraded because of a reduced current drop, if not totally destroyed due to microwave oscillations or avalanche breakdown in the anode region. The computer simulations have also shown that the presence of a large doping notch close to one of the contacts will similarly destroy the bistable switching by eliminating the current drop or by causing instability problems. As a

last theoretical consideration, a hysteresis effect in the I-V curve is discussed in relation to the diode length. The computer simulations show that the domain sustaining voltage is smaller than the threshold voltage. Thus, when the voltage is reduced across the device, it will switch back to an off-state current, that is lower than the threshold current, even when the load resistance is infinitely small. This hysteresis effect will be smaller in a short device, because the minimum voltage the anode domain can absorb is independent of the diode length and therefore will amount to a larger fraction of the threshold voltage in a shorter device.

III. EXPERIMENTAL RESULTS

A. Material and Contact Properties

The TED's used in the present work had n$^+$-n-n$^+$ sandwich layers grown by liquid phase epitaxy on n$^+$-substrates. Active layer thicknesses and doping densities were about 5–15 μm and 1–7 $\times$ 10^{15} cm^{-3}, respectively. Owing to the growth procedure, a doping profile increasing towards the substrate but with a gradient below 30 percent was normally found when the active layers were profiled. In the following we refer to positive polarity when the substrate is positive, negative polarity when the substrate is negative. This definition, combined with the definition of positive or negative gradients in Section II, implies that positive (negative) polarity goes together with positive (negative) gradients for the devices used. However, some devices had such a small gradient that these distinctions became meaningless.

B. Circuitry and Stability Check

In the initial experiments packaged devices were mounted in a 7-mm coaxial air line and operated into a series resistive load. Current and voltage waveforms for the packaged devices were displayed on an 18-GHz sampling scope. In this way switching times could be measured and it could also be checked that no microwave oscillations were present. The frequency response of the coaxial mount and the surrounding circuitry was found satisfactory up to 18 GHz. Further details of this setup and the results obtained have been reported elsewhere [9].

In order to improve the sensitivity of the stability check and reduce mounting parasitics, which tend to degrade the observed switching speed, later work was carried out using an even cleaner microwave circuit. TED chips were shunt mounted in a 50-Ω microstrip line placed in an 18-GHz test fixture [10]. The voltage across the chip was monitored directly with the 18-GHz sampling scope, allowing shorter switching times and weaker microwave oscillations—if any—to be observed.

C. Current Drops

In Fig. 8 the relative current drops are plotted versus doping densities. Points measured with positive polarity
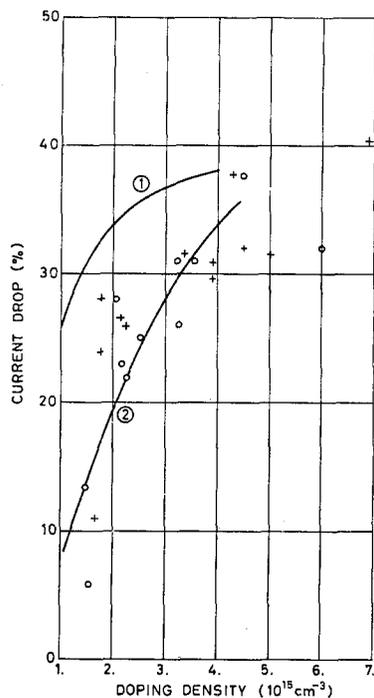
Fig. 8.   Measured and calculated current drop versus doping density. Curve 1: Large-signal computer calculations. Curve 2: Simple, analytical model [4]. + Measured in positive polarity. o Measured in negative polarity.

Fig. 9.   Typical recorded voltage waveform for bare-mounted Gunn switch in 18-GHz microstrip circuit. Device data: $L_a = 10 \ \mu m$, $n_0 = 4.5 \times 10^{15}$ cm^{-3}, $R_0 = 4 \ \Omega$, $T_0 = 300$ K.

are indicated by +, negative by O. Curve 1 applies for large-signal computer simulations, curve 2 for the earlier analytical model [4]. All experimental points apply for low-duty-cycle pulsed operation where no heating is involved, and this is true for the theoretical curves as well.

The trend predicted by the theoretical work, that the current drop should increase with the doping density, is clearly confirmed experimentally. The maximum experimental current drop is 41.5 percent [9] in good agreement with extrapolated theoretical results. At first glance the simple analytical model agrees closest with experimental results, while the computer simulations at lower doping levels tend to give too optimistic results. This is because a flat and smooth doping profile was used in the computer simulations, so the apparent discrepancy could be removed by introducing doping gradients and random fluctuations in the profile, as can be anticipated from Fig. 6. In Fig. 8 there is no clear dependence of the current drop on the polarity, and this agrees well with Fig. 7, where only a weak and, in practice, insignificant dependence was suggested. Apart from the current drop it was found that devices in positive polarity (i.e., increasing profile towards anode) were more prone to microwave oscillations, in negative polarity to impact ionization. These two conclusions are easily interpreted using the computer simulations in Section II. Positive polarity gives cathode-triggered oscillations, negative polarity anode domains with high peak fields.

Since most possible applications of Gunn switches would involve heavy duty cycle, it is important to avoid
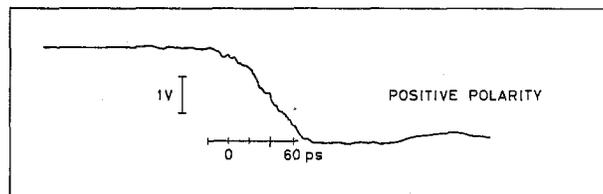
excessive device heating, which otherwise would reduce the off-state peak current to the point, where the current drop is almost eliminated. Therefore, the detrimental effect of device heating has been investigated in heavy-duty-cycle experiments. The devices were mesa-etched, mounted with substrate towards the heat sink, and had a length of 6 μm—an optimum length as will be discussed later. Three groups of devices were tested, having doping levels around 6.8, 4.3, and 3.9 $\times$ 10^{15} cm^{-3}, respectively. For the most lightly doped devices, the relative current drop decayed slowest with increasing duty cycle. For the doping 3.9 $\times$ 10^{15} cm^{-3} a current drop of 25 percent remained at 30-percent duty cycle, corresponding to the temperature increase encountered in CW operation of the same device being flip-chip mounted. Hence it is realistic to expect that useful current drops will remain in CW operation when such devices are used.

D. Switching Time

Using packaged devices in the coaxial circuit, switching times down to 100 ps were observed, but the computer simulations in Section II predicted substantially shorter switching times. Now, considering typical values for the series inductance and parallel capacitance of the package, a simple calculation has shown the observed switching time to be limited by the package, not by the Gunn switch itself. This conclusion was experimentally confirmed by the 60-ps switching times observed from TED chips mounted in the microstrip circuit. An example is given in Fig. 9, where the chip voltage jump for the switch-on is recorded versus time. The device was 10 μm long, doped to 4.5 $\times$ 10^{15} cm^{-3}, had a doping profile believed to rise about 20 percent towards the substrate, and the device was operated in positive polarity.

Devices having larger doping gradients (> 50 percent, for example) and being operated in negative polarity tended to have much longer switching times and much "softer" threshold voltages for the switch-on. With reference to the computer simulations in Section II, this behavior may be interpreted as follows. When the doping gradient is large and negative, the fast and abrupt switch-on caused by the absolute anode instability shown in Figs. 4 and 5 does not prevail. Instead, a smaller anode domain is already formed below threshold, and this contributes an extra domain capacitance, which in turn gives a longer RC time constant and softer threshold voltage for the switch-on.

E. Optimum Device Parameters

The optimum device parameters for the bistable switch will now be discussed.

The doping density n_0 should be high to give a high current drop. On the other hand, ionization and heating problems become more severe with higher doping, so, with reference to Fig. 8, a good compromise of 3–4 × 10^{15} cm^{-3} is arrived at.

The length of the active layer L_a should be short in order to provide for a low operating voltage, improved thermal performance, and reduced hysteresis in the *I–V* curve. On the other hand, the length is downward limited by the anode domain, so the optimum length will be about 6 μm.

The area A is determined by thermal considerations and by the required current modulation ΔI for the specific application in question. Having chosen the optimum doping n_0 and thereby the relative current drop $\Delta I/I_T$ from Fig. 8, curve 2, for example, A is given by

$$A = \frac{\Delta I}{(\Delta I/I_T)E_T q n_0 \mu_0}$$

where μ_0 is the low field mobility.

IV. CONCLUSION AND DISCUSSION

In summary the computer simulations have identified three switching modes all leading to a stable anode domain: 1) cathode-triggered traveling domain; 2) cathode-triggered accumulation layer; and 3) anode-triggered domain. Moreover, current drops up to 40 percent and switching times down to 30 ps have been predicted. In the interest of simplicity, relaxation effects have been neglected in the computer simulations, which also contain an oversimplified treatment of the high field anode n/n$^+$-interface, for which a correct theoretical treatment is extremely difficult if possible at all. Because of these simplifications, all predictions have been closely compared with experimental results.

In the experiments, bistable switching with current drops up to 40 percent and switching times down to 60 ps have been obtained in low-duty-cycle operation with threshold currents typically around 400 mA. High-duty-cycle pulsed experiments with "mesa-up" devices indicated that CW operation with current drops in excess of 25 percent should be possible with flip-chip mounted devices. Optimum devices should be doped in the 3–4 × 10^{15} cm^{-3} range, be about 6 μm long, have smooth doping profiles with gradients below 20 percent, and should have high quality interfaces. Mounting procedures with even smaller parasitics may reduce the experimental switching time below 60 ps.

Bistable Gunn switches offer the advantages of fast switching with large relative current drops at high current levels, and they are capable of pulse sharpening in the sense that a slow trigger pulse gives fast switching. Their limitations are the hysteresis effect in the switch-off, tendency to microwave oscillations when operated into a low series resistance, and the fact that they are two-terminal and not three-terminal devices.

The Gunn switches have potentials as ultrafast pulse sharpeners and logic elements [11] in, for example, gigabit/second PCM communication systems, and they have been investigated as modulators for semiconductor lasers in optical fiber communication [12]. In these applications they will, however, meet competition from the Schottky-barrier-triggered three-terminal Gunn switch [13], [14] and the GaAs Schottky-barrier FET [15], [16]. Finally, it should be noted that the present work, in addition to assessing the potentials of the bistable Gunn switch, contributes to the understanding of heavily doped transferred electron oscillators and amplifiers having low cathode fields. This is so because in such devices high field anode domains [3] are of central importance for the bandwidth, noise, thermal behavior, and failure mode.

APPENDIX A
NUMERICAL INTEGRATION OF TIME-DEPENDENT EQUATIONS

Let L_t denote the total length of the diode including both contacts. The total current density given by

$$J(t) = \frac{1}{L_T} \int_0^{L_t} \left[qnv - q\frac{\partial}{\partial x}(Dn) + \epsilon \frac{\partial E}{\partial t} \right] dx \quad \text{(A1)}$$

can be divided into the electronic current density given by

$$J_e(t) = \frac{q}{L_t} \int_0^{L_t} \left[nv - \frac{\partial}{\partial x}(Dn) \right] dx \quad \text{(A2)}$$

and the capacitive current density given by

$$J_c(t) = \frac{\epsilon}{L_t}\frac{dV}{dt} \quad \text{(A3)}$$

where the device voltage $V(t)$ is equal to the dictated (constant or time varying) source voltage, because zero source impedance is assumed.

For a doping profile $n_D(x)$ equaling n_0 in the active layer and exceeding n_0 by more than an order of magnitude in the heavily doped contacts, $n_D(x)$ should be substituted for n_0 in (1). Then elimination of $n(x,t)$ from (1) and (2) gives

$$\frac{\partial E}{\partial t} = \frac{q}{\epsilon}\left[\frac{J(t)}{q} - \left(v - \frac{\partial D}{\partial x}\right)\left(n_D + \frac{\epsilon}{q}\frac{\partial E}{\partial x}\right) \right.$$
$$\left. + D\left(\frac{dn_D}{dx} + \frac{\epsilon}{q}\frac{\partial^2 E}{\partial x^2}\right) \right]. \quad \text{(A4)}$$

Now, L_t is divided into P intervals each of length $\Delta x = L_t/P$, and the time into intervals each of duration Δt. Hence

$$x = X\Delta x, \qquad X = 0,1,2,\cdots,P$$

and

$$t = T\Delta t, \qquad T = 0,1,2,\cdots.$$

For sufficiently small values of Δx and Δt, differential equation

$$E(X,T) = E(X,T-1) + \frac{q}{\epsilon}\Delta t\left\{\frac{J(T-1)}{q} - \left[v(X,T-1) - \frac{D(X+1,T-1)-D(X-1,T-1)}{2\Delta x}\right] \times \left[n_D(X)\right.\right.$$

$$\left. + \frac{\epsilon}{q}\frac{E(X+1,T-1)-E(X-1,T-1)}{2\Delta x}\right] + D(X,T-1)\left[\frac{n_D(X+1)-n_D(X-1)}{2\Delta x}\right.$$

$$\left.\left. + \frac{\epsilon}{q}\frac{E(X+1,T-1)-2E(X,T-1)+E(X-1,T-1)}{(\Delta x)^2}\right]\right\} \quad (A5)$$

where abbreviations such as $E(X,T) = E(X\Delta x, T\Delta t)$ and $D(X,T) = D[E(X,T)]$ have been used. Equation (A5) allows the determination of the new E values using the old ones on the right side.

The boundary conditions for the n+-cathode are $n(0,T) = n_D(0)$ and

$$E(0,T) = \frac{J(T)}{q n_D(0)\mu_c}. \quad (A6)$$

Similarly, the boundary conditions for the n+-anode are $n(P,T) = n_D(P)$ and

$$E(P,T) = \frac{J(T)}{q n_D(P)\mu_c}. \quad (A7)$$

Here the mobility in the contacts μ_c is taken to be one half the low field mobility μ_0, since this is more realistic and because the increased dielectric relaxation time permits the use of larger Δt and Δx values.

Given $J(T)$, the numerical integration now proceeds as follows.

1) $E(X,T)$, $X = 0,1,2,\cdots,P$ is calculated from (A5)–(A7).

2) Any discrepancy between the integrated field and $V(T)$ is removed by correcting the field profile to

$$E(X,T)$$

$$+ \left[V(T) - \Delta x \sum_{X'=1}^{P} E(X',T)\right]\Big/L_t, \quad X = 0,1,2,\cdots,P.$$

3) The electron density profile is calculated from the Poisson equation (1):

$$n(X,T) = n_D(X)$$

$$+ \frac{\epsilon}{q}\frac{E(X+1,T)-E(X-1,T)}{2\Delta x}, \quad X = 1,2,\cdots,P-1.$$

4) The electronic current density is calculated from (A2):

$$J_e(T) = \frac{q\Delta x}{L_t}\sum_{X=1}^{P}\left[n(X,T)v(X,T)\right.$$

$$\left. - \frac{D(X,T)n(X,T)-D(X-1,T)n(X-1,T)}{\Delta x}\right].$$

5) The new total current density is calculated with good approximation from (A1)–(A3):

$$J(T+1) = J_e(T) + \frac{\epsilon}{L_t}\frac{V(T+1)-V(T)}{\Delta t}.$$

Substituting $T+1$ for T in (A5)–(A7), the calculations are continued by repeating the entire procedure. Compared to an integration scheme used earlier [17], this new method is advantageous because it ensures the satisfaction of the anode boundary conditions.

APPENDIX B
NUMERICAL INTEGRATION OF TIME-INDEPENDENT EQUATIONS

Setting $\partial/\partial t$ terms equal to zero in Poisson equation (1) and continuity equation (2), substituting $n_D(x)$ for n_0 in (1), and eliminating $n(x)$ from (1) and (2) gives

$$\frac{d^2E}{dx^2} = \frac{q}{\epsilon}\left[\frac{\left(v - \frac{dD}{dx}\right)\left(n_D + \frac{\epsilon}{q}\frac{dE}{dx}\right) - \frac{J}{q}}{D} - \frac{dn_D}{dx}\right]$$

For sufficiently small Δx values this differential equation can be approximated by the difference equation

$$E(X) = \frac{E(X+1)+E(X-1)}{2} - \frac{q}{2\epsilon}(\Delta x)^2$$

$$\times \left\{\frac{\left[v(X) - \frac{D(X+1)-D(X-1)}{2\Delta x}\right]\left[n_D(X) + \frac{\epsilon}{q}\frac{E(X+1)-E(X-1)}{2\Delta x}\right] - \frac{J}{q}}{D(X)}\right.$$

$$\left. - \frac{n_D(X+1)-n_D(X-1)}{2\Delta x}\right\}. \quad (B1)$$

The boundary conditions for the n^+-cathode are $n(0) = n_D(0)$ and

$$E(0) = \frac{J}{qn_D(0)\mu_c}. \tag{B2}$$

Similarly, the boundary conditions for the n^+-anode are $n(P) = n_D(P)$ and

$$E(P) = \frac{J}{qn_D(P)\mu_c}. \tag{B3}$$

The numerical integration involves an iterative procedure. As the stable field profile for a fixed device voltage is independent of any source impedance that might be present, a resistor $R_G = 50\ \Omega$ was introduced in series with the source voltage V_G in order to improve the convergence of the iterative method. The device and source voltages are then related according to

$$V = V_G - R_G A J \tag{B4}$$

where A is the cross-sectional area of the diode.

Having guessed a J value, calculated the corresponding V value from (B4) and guessed a field profile that satisfies the boundary conditions (B2) and (B3), the numerical integration proceeds as follows.

1) A new field profile $E(X)$, $X = 0,1,2, \cdots , P$ is calculated from (B1)–(B3).

2) If the integrated field deviates more than 0.1 percent from V, then V is corrected to

$$\frac{1}{2}\left[V + \Delta x \sum_{X=1}^{P} E(X) \right]$$

a new current density is calculated from

$$J = \left[V_G - \frac{1}{2}(V + \Delta x \sum_{X=1}^{P} E(X)) \right]\bigg/(AR_G)$$

and with those new V and J values the procedure is repeated.

3) When the integrated field deviates less than 0.1 percent from V, the iterative procedure is terminated and the electron density profile is calculated from the

Poisson equation

$$n(X) = n_D(X) + \frac{\epsilon}{q}\frac{E(X+1) - E(X-1)}{2\Delta x},$$

$$X = 1,2, \cdots ,P-1.$$

REFERENCES

[1] H. W. Thim, "Stability and switching in overcritically doped Gunn-diodes," *Proc. IEEE* (Lett.), vol. 59, pp. 1285–1286, Aug. 1971.
[2] H. W. Thim, "Experimental verification and bistable switching with Gunn-diodes," *Electron. Lett.*, vol. 7, pp. 246–247, May 1971.
[3] P. Jeppesen, B. Jeppsson, and P. Jøndrup, "A broadband negative conductance GaAs TED," *Proc. IEEE* (Lett.), vol. 63, pp. 1364–1365, Sept. 1975.
[4] P. Jeppesen and B. Jeppsson, "A simple analysis of the stable field profile in the supercritical TEA," *IEEE Trans. Electron Devices*, vol. ED-20, pp. 371–379, Apr. 1973.
[5] D. E. McCumber and A. G. Chynoweth, "Theory of negative-conductance amplification and Gunn instabilities in "two-valley" semiconductors," *IEEE Trans. Electron Devices*, vol. ED-13, pp. 4–21, Jan. 1966.
[6] J. Magarshack, A. Rabier, and R. Spitalnik, "Optimum design of transferred electron amplifier devices in GaAs," *IEEE Trans. Electron Devices* (Corresp.), vol. ED-21, pp. 652–654, Oct. 1974.
[7] J. A. Copeland and S. Knight, "Applications utilizing bulk negative resistance," in *Semiconductors and Semimetals*, vol. 7A, R. K. Willardson and A. C. Beer, Ed., New York: Academic, pp. 3–72, 1971.
[8] P. Guéret, "Convective and absolute instabilities in semiconductors exhibiting negative differential mobility," *Phys. Rev. Lett.*, vol. 27, pp. 256–257, Aug. 1971.
[9] S. H. Izadpanah, B. Jeppsson, P. Jeppesen, and P. Jøndrup, "A high current drop GaAs bistable switch," *Proc. IEEE* (Lett.), vol. 62, pp. 1166–1167, Aug. 1974.
[10] P. Jøndrup, "A theoretical and experimental investigation of the bistable switching in supercritical n^+nn^+ GaAs TEDs," Ph.D. dissertation, LD 27, Electromagnetics Institute, Technical University of Denmark, July 1975.
[11] S. H. Izadpanah, "Pulse generation and processing with GaAs bistable switches," *Solid State Electronics*, vol. 19, pp. 129–132, 1976.
[12] H. W. Thim, L. R. Dawson, J. V. DiLorenzo, J. C. Dyment, C. J. Hwang, and D. L. Rode, "Subnanosecond PCM of GaAs lasers by Gunn-effect switches," *Digest of 1973 IEEE ISSCC*, pp. 92–93, Feb. 1973.
[13] K. Mause, A. Schlachetzki, E. Hesse, and H. Salow, "Gunn device gigabit rate digital microcircuits," *IEEE J. Solid-State Circuits*, vol. SC-10, pp. 2–12, Feb. 1975.
[14] H. Yanai, M. Yano, and T. Kamiya, "Direct modulation of a double-heterostructure laser using a Schottky-barrier-gate Gunn-effect digital device," *IEEE J. Quantum Electron.*, vol. QE-11, pp. 519–524, July 1975.
[15] R. L. van Tuyl and C. A. Liechti, "High-speed integrated logic with GaAs MESFET's," *IEEE J. Solid-State Circuits*, vol. SC-9, pp. 269–276, Oct. 1974.
[16] V. Ostoich, P. Jeppesen, and N. Slaymaker, "Direct modulation of D.H. GaAlAs lasers with GaAs MESFET's," *Electron. Lett.*, vol. 11, pp. 515–516, Oct. 1975.
[17] P. Jeppesen and B. Jeppsson, "LSA relaxation oscillator principles," *IEEE Trans. Electron Devices*, vol. ED-18, pp. 439–449, July 1971.